

# Crystal Structure and Function of 5-Formaminoimidazole-4-carboxamide Ribonucleotide Synthetase from *Methanocaldococcus jannaschii*<sup>†,‡</sup>

Yang Zhang,<sup>§</sup> Robert H. White,<sup>||</sup> and Steven E. Ealick<sup>\*,§</sup>

Department of Chemistry and Chemical Biology, Cornell University, Ithaca, New York 14853-1301, and Department of Biochemistry, Virginia Polytechnic Institute and State University, Blacksburg, Virginia 24061-0308

Received July 17, 2007; Revised Manuscript Received October 3, 2007

**ABSTRACT:** Purine biosynthesis requires 10 enzymatic steps in higher organisms, while prokaryotes require an additional enzyme for step 6. In most organisms steps 9 and 10 are catalyzed by the *purH* gene product, a bifunctional enzyme with both 5-formaminoimidazole-4-carboxamide ribonucleotide (FAICAR) synthase and inosine monophosphate (IMP) cyclohydrolase activity. Recently it was discovered that Archaea utilize different enzymes to catalyze steps 9 and 10. An ATP-dependent FAICAR synthetase is encoded by the *purP* gene, and IMP cyclohydrolase is encoded by the *purO* gene. We have determined the X-ray crystal structures of FAICAR synthetase from *Methanocaldococcus jannaschii* complexed with various ligands, including the tertiary substrate complex and product complex. The enzyme belongs to the ATP grasp superfamily and is predicted to use a formyl phosphate intermediate formed by an ATP-dependent phosphorylation. In addition, we have determined the structures of a PurP orthologue from *Pyrococcus furiosus*, which is functionally unclassified, in three crystal forms. With approximately 50% sequence identity, *P. furiosus* PurP is structurally homologous to *M. jannaschii* PurP. A phylogenetic analysis was performed to explore the possible role of this functionally unclassified PurP.

The purine biosynthetic pathway generates inosine monophosphate, which is subsequently converted to either adenosine monophosphate or guanosine monophosphate. Buchanan worked out the details of the vertebrate pathway in the 1950s, identifying 10 enzymatic conversions (1). Later, Stubbe and co-workers showed that in prokaryotes the conversion of aminoimidazole ribonucleotide to carboxyaminoimidazole ribonucleotide catalyzed by PurE in step 6 requires an additional enzyme (PurK)<sup>1</sup> (2–4), resulting in a total of 11 enzymatic conversions. In *Escherichia coli* each step of the pathway is catalyzed by a monofunctional enzyme, with the exception of the last two steps, while in vertebrates steps 2 (PurD), 3 (PurN), and 5 (PurM) comprise

a trifunctional enzyme (5), steps 6 (PurE) and 7 (PurC) comprise a bifunctional enzyme (6, 7), and steps 9 and 10 are catalyzed by the bifunctional enzyme PurH (8–11). Additional species-dependent gene fusions have been observed.

Other deviations from the vertebrate purine biosynthetic pathway have also been observed. In vertebrates, formyltransferase reactions occur in steps 3 (PurN) and 9 (PurH), with *N*<sup>10</sup>-formyltetrahydrofolate as the donor. However, some Archaea lacking tetrahydrofolate as a cofactor utilize an ATP-dependent formate ligation: PurT for step 3 (12–14) and PurP for step 9 (15). Both the tetrahydrofolate-dependent and ATP-dependent formyltransferase reactions are found in *E. coli* (12). In vertebrates, PurH catalyzes step 10, while in methanogenic bacteria PurO, which is structurally dissimilar to PurH (9, 11), catalyzes step 10 (16, 17). Examination of the available genomes suggests that other variations in the purine biosynthetic pathway remain to be discovered.

Enzyme structures for all of the known purine biosynthetic activities have been determined with the exception of PurP, which converts aminocarboxyimidazole ribonucleotide (AICAR) to formylaminocarboxyimidazole ribonucleotide (FAICAR) in step 9. PurP from *Methanocaldococcus jannaschii* has been biochemically characterized (15), and sequence comparisons indicate the presence of PurP orthologues in a number of related organisms. Sequence comparisons reveal that PurP is a member of the ATP grasp superfamily (18–20). The purine biosynthetic enzymes PurD, PurT, PurK, and PurC are also members of the ATP grasp superfamily (14, 21–24).

<sup>†</sup> This work was supported by National Institutes of Health Grants RR15301 and GM073220 and the National Science Foundation Grant MCB0231319 to R.H.W. S.E.E. is indebted to the W. M. Keck Foundation and the Lucille P. Markey Charitable Trust.

<sup>‡</sup> The Brookhaven Protein Data Bank codes are 2R7K, 2R7L, 2R7M, 2R7N, 2R84, 2R85, 2R86, and 2R87.

<sup>\*</sup> To whom correspondence should be addressed. Phone: (607) 255-7961. Fax: (607) 255-1227. E-mail: see3@cornell.edu.

<sup>§</sup> Cornell University.

<sup>||</sup> Virginia Polytechnic Institute and State University.

<sup>1</sup> Abbreviations: AICAR, 5-aminoimidazole-4-carboxamide 5'-monophosphate ribonucleotide; FAICAR, 5-formaminoimidazole-4-carboxamide 5'-monophosphate ribonucleotide; PurP, FAICAR synthetase and AICAR transformylase; PurO, IMP cyclohydrolase; PurD, glycylamide ribonucleotide synthetase; PurT, phosphoribosylglycinamide transformylase; PurK, *N*<sup>5</sup>-carboxyaminoimidazole ribonucleotide synthetase; PurC, phosphoribosylaminoimidazolesuccinocarboxamide synthetase; PurH, bifunctional AICAR transformylase and IMP cyclohydrolase; FGAR, formylglycinamide ribonucleotide; PurL, FGAR amidotransferase; FGAM, formylglycinamide ribonucleotide; AIR, aminoimidazole ribonucleotide; PurM, AIR synthetase; au, asymmetric unit; rmsd, root mean square deviation; MPD, 2-methyl-2,4-pentanediol.

Here we report the structure of PurP from *M. jannaschii* (MjPurP) complexed with substrates, products, and analogues. Among the ATP grasp members MjPurP shows a novel hexameric arrangement in which loops from 3-fold-related monomers fold over onto adjacent monomers. The ATP binding site of PurP is similar to those for other members of the ATP grasp superfamily. The AICAR/FAICAR binding site is comprised of the conserved residues His27, Arg264, Ser266, and Arg314. We also report structures from three crystal forms of a Pf1517 (PfPurP), one of two PurP orthologues found in *Pyrococcus furiosus*. Although the MjPurP and PfPurP active sites are highly conserved, and PfPurP binds both ATP and AICAR, PfPurP does not catalyze the FAICAR synthetase reaction, and its function remains unknown. A phylogenetic analysis of PurP orthologues is also presented.

## MATERIALS AND METHODS

**Overexpression and Purification of MjPurP.** *M. jannaschii* purP gene Mj0136 was cloned into the expression vector pET19b and overexpressed in *E. coli* B834(DE3), a methionine auxotrophic strain (15). For overexpression of native protein, cells were grown in LB medium supplemented with 100  $\mu$ g/mL ampicillin. For overexpression of selenomethionine (SeMet)-substituted protein, cells were grown in M9 minimal salts supplemented with 4% (w/v) glucose, 2 mM MgSO<sub>4</sub>, 0.1 mM CaCl<sub>2</sub>, 1% BME vitamin solution (Gibco-BRL), 25  $\mu$ g/mL FeSO<sub>4</sub>·7H<sub>2</sub>O, and a 40  $\mu$ g/mL concentration of each of the L-amino acids (L-selenomethionine substitutes for L-methionine). The cells were induced with 0.1 mM isopropyl  $\beta$ -D-thiogalactoside (IPTG) for 6 h at 25 °C once the absorbance of the cell culture reached an OD<sub>600</sub> of 0.8. The recombinant protein was purified by metal-chelate affinity chromatography using a cobalt column (Clontech). Polyhistidine-tagged MjPurP was eluted from the column with buffer A (50 mM sodium phosphate, pH 7.0, 300 mM NaCl, 1 mM  $\beta$ -mercaptoethanol, and 300 mM imidazole). The fractions containing MjPurP were combined and exchanged into 10 mM Tris-HCl, pH 7.6, 1 mM MgCl<sub>2</sub>, and 1 mM dithiothreitol. For the native protein, 1 L of cell culture produced ~20 mg of homogeneous MjPurP, while for the SeMet protein, only 2 mg of MjPurP/L of cell culture was obtained. The purified protein was then concentrated to 10 mg/mL using 10 kDa cutoff microcon concentrators (Amicon).

**Overexpression and Purification of PfPurP.** *P. furiosus* purP gene at locus Pf1517 was amplified by PCR from genomic DNA and subcloned into the pT7-7 vector. The gene-containing plasmid was overexpressed in *E. coli* BL21(DE3). The cells were grown in LB medium in the presence of 100  $\mu$ g/mL ampicillin at 37 °C until the absorbance of the cell culture reached an OD<sub>600</sub> of 0.8, at which point the cells were induced with 0.2 mM IPTG for an additional 6 h at 25 °C. The cells were harvested by centrifugation and sonicated on ice in buffer B (20 mM Tris-HCl, pH 7.5). The crude cell extract was prepurified by heating in a water bath at 70 °C for 30 min, followed by centrifugation at 15000g for 20 min to remove the insoluble material. Heat-stable cell extract was applied to a MonoQ HR anion exchange column (1  $\times$  10 cm). After the column was washed with 15 column volumes of buffer B, the bound protein was

eluted with a 15 column volume linear gradient from 0 to 1 M NaCl in buffer B at a flow rate of 0.4 mL/min. The fraction containing homogeneous PfPurP was buffer exchanged into 10 mM Tris-HCl, pH 7.5, and 2 mM MgCl<sub>2</sub> and concentrated to 15 mg/mL.

**Crystallization of MjPurP.** Crystallization was performed using the hanging drop vapor diffusion method at 18 °C with drops containing 1.5  $\mu$ L of protein solution and 1.5  $\mu$ L of reservoir solution. MjPurP was subjected to a series of sparse matrix screens (Hampton Research, Emerald Biostructures) to determine initial crystallization conditions. Both SeMet and native protein crystallized from 1.2–1.4 M (NH<sub>4</sub>)<sub>2</sub>SO<sub>4</sub>, 0.2 M NaCl, and 0.1 M sodium acetate at pH 4.1–4.3. To obtain the ligand-complexed structures, ATP, AMPPCP, ADP, AMP, AICAR, and FAICAR were used for cocrystallization with MjPurP at 1 mM concentration for FAICAR and 5 mM for the others. The FAICAR was prepared by the enzymatic formylation of AICAR with ATP and formate catalyzed by MjPurP followed by purification of the FAICAR on a MonoQ column, while all other compounds were purchased from Sigma-Aldrich. Crystals, in the shape of rhombohedral prisms, usually appear in a week and reach a maximum size of 300  $\mu$ m  $\times$  300  $\mu$ m  $\times$  80  $\mu$ m in two weeks. These crystals belong to the space group R32 with unit cell dimensions of  $a = 109.2$  Å and  $c = 255.7$  Å on average. Each asymmetric unit (au) contains one protomer, corresponding to a solvent content of 65% and Matthews coefficient (25) of 3.5 Å<sup>3</sup>/Da.

The soaking experiments were performed at 18 °C for 1 h. The stabilizing solution contains 1.5 M (NH<sub>4</sub>)<sub>2</sub>SO<sub>4</sub>, 0.2 M NaCl, 20 mM MgCl<sub>2</sub>, and 0.1 M sodium acetate at pH 4.1. The ligand concentration in the soaking solutions was 50 mM for ATP, AMPPCP, ADP, and AMP, 20 mM for AICAR, and 6 mM for FAICAR. For the AMPPCP-AICAR complex, 20 mM ammonium formate was also present in the solution.

**Crystallization of PfPurP.** The crystallization experiment for PfPurP was similar to those for MjPurP. PfPurP crystallized in three crystal forms. The first crystal form grew from 30–32% 2-methyl-2,4-pentanediol (MPD), 200 mM NaCl, and 100 mM Tris-HCl, pH 7.0. Crystals usually appear in 2 days and reach a maximum size of 200  $\mu$ m  $\times$  200  $\mu$ m  $\times$  80  $\mu$ m in one week. The crystals are in the shape of rhombohedral prisms and belong to the space group R32. The unit cell dimensions are  $a = 123.4$  Å and  $c = 375.5$  Å. Each au contains two protomers, corresponding to a solvent content of 65% and Matthews coefficient of 3.5 Å<sup>3</sup>/Da.

A second crystal form was obtained from 30–35% MPD and 100 mM Na<sup>+</sup>/K<sup>+</sup> phosphate, pH 6.2, in the presence of 10 mM ATP. This crystal form belongs to the space group R32 with unit cell dimensions of  $a = 122.5$  Å and  $c = 560.9$  Å. In this crystal form, there are also two protomers in the au, corresponding to a solvent content of 76% and Matthews coefficient of 5.2 Å<sup>3</sup>/Da.

The third PfPurP crystal form grew from 10% (v/v) 2-propanol, 200 mM Li<sub>2</sub>SO<sub>4</sub>, and 100 mM sodium phosphate-citrate at pH 4.2, in the presence of 5 mM ADP. The crystals are in the space group P2<sub>1</sub> with unit cell dimensions of  $a = 75.7$  Å,  $b = 126.8$  Å,  $c = 121.4$  Å, and  $\beta = 102.9^\circ$ . There are six protomers in the au, corresponding to a solvent content of 51% and Matthews coefficient of 2.5 Å<sup>3</sup>/Da.

Table 1: Data Collection Statistics<sup>a</sup>

protein complex	<i>Mj</i> PurP AICAR— AMPPCP (SeMet)	<i>Mj</i> PurP AICAR— AMPPCP	<i>Mj</i> PurP AICAR— ATP	<i>Mj</i> PurP FAICAR— ADP	<i>Mj</i> PurP AMP— AMP	<i>Pf</i> PurP AICAR— AMP	<i>Pf</i> PurP AMP— AMP	<i>Pf</i> PurP Pi—ATP	<i>Pf</i> PurP Pi—ADP
wavelength (Å)	0.979 22	0.979 22	0.979 22	0.979 22	0.979 22	0.979 18	0.979 18	0.979 18	0.917 70
resolution (Å)	2.5	2.1	2.1	2.4	2.3	1.9	1.7	2.5	2.3
space group	<i>R</i> 32	<i>R</i> 32	<i>R</i> 32	<i>R</i> 32	<i>R</i> 32	<i>R</i> 32	<i>R</i> 32	<i>R</i> 32	<i>P</i> 2 <sub>1</sub>
unit cell									
<i>a</i> (Å)	109.5	109.4	109.6	108.0	109.4	123.7	123.2	122.5	75.7
<i>b</i> (Å)									126.8
<i>c</i> (Å)	256.2	256.0	255.8	254.3	256.3	375.4	376.3	560.9	121.4
β (deg)									102.9
total no. of reflns	401 282	557 779	161 067	103 716	140 027	602 085	834 589	420 106	288 596
no. of unique reflns	20 490	34 334	31 509	20 897	26 365	85 987	119 607	55 984	95 364
completeness (%)	98.0 (82.3)	98.5 (90.7)	90.3 (61.6)	92.0 (57.4)	99.6 (100)	99.3 (94.4)	99.0 (97.0)	97.9 (81.9)	96.7 (99.0)
<i>R</i> <sub>sym</sub> <sup>b</sup> (%)	9.7 (25.0)	7.9 (28.0)	5.4 (14.6)	7.9 (23.4)	6.8 (36.4)	7.4 (36.5)	5.2 (28.4)	5.7 (28.3)	7.6 (24.3)
<i>I</i> /σ	42.2 (6.8)	37.6 (7.8)	26.1 (5.6)	21.0 (3.7)	28.0 (4.4)	25.0 (3.0)	36.6 (3.9)	32.0 (3.0)	15.5 (4.5)
redundancy	19.6 (12.6)	16.2 (11.4)	5.1 (4.6)	5.0 (3.9)	5.3 (4.7)	7.0 (5.9)	7.0 (6.0)	7.5 (6.1)	3.0 (2.9)

<sup>a</sup> Values for the highest resolution shell are given in parentheses. <sup>b</sup>  $R_{\text{sym}} = \sum_i |I_i - \langle I \rangle| / \sum_i I_i$ , where  $\langle I \rangle$  is the mean intensity of the *N* reflections with intensities *I<sub>i</sub>* and common indices *h*, *k*, and *l*.

**X-ray Intensity Measurements.** For cryoprotection, the *Mj*PurP crystals were briefly transferred into a buffer containing 12% glycerol, 12% ethylene glycol, 1.6 M (NH<sub>4</sub>)<sub>2</sub>-SO<sub>4</sub>, 0.2 M NaCl, and 0.1 M sodium acetate at pH 4.1. The crystals were then flash frozen by plunging them into liquid nitrogen. The *Pf*PurP crystals in both *R*32 forms were directly frozen without cryoprotection, while those in monoclinic form were cryoprotected by 15% glycerol added to the mother liquor. Data sets were collected either at Advanced Photon Source (APS) beamline 24-ID-C using an ADSC Quantum 315 detector or at Cornell High Energy Synchrotron Source (CHESS) beamline F1 using an ADSC Quantum 270 detector. For the single-wavelength SeMet data set of *Mj*PurP, the energy was selected to maximize Δ*f*'' of the incorporated selenium, and a total of 360° of data were collected. A total of 90–150° of data were collected for each of the other data sets. The oscillation per image ranged from 0.5° to 1°, depending on the mosaicity of the crystal. The crystals of *Mj*PurP diffracted to around 2.0 Å; however, the diffraction pattern was usually anisotropic, resulting in low completeness in the high-resolution shells. The crystals of *Pf*PurP diffracted to 1.7–1.9 Å for the crystal form of *R*32 in the small unit cell, 2.5 Å for *R*32 in the large unit cell, and 2.3 Å for the *P*2<sub>1</sub> crystal form. The HKL2000 suite of programs was used for integration and scaling (26). Data processing statistics are summarized in Table 1.

**Structure Determination and Refinement.** To determine the structure of *Mj*PurP, single-wavelength anomalous dispersion (SAD) phasing, density modification, and automatic model building were performed at 2.5 Å using the program autoSHARP (27). Approximately 300 out of a total of 361 residues were built with correct side chains in the initial model, which was manually adjusted and further completed using the interactive graphics program Coot (28). The model refinement was performed through alternating cycles of manual rebuilding using Coot and restrained refinement using CNS (29) and Refmac5 (30). The native data set of *Mj*PurP complexed with AMPPCP–AICAR at 2.1 Å was used to extend the phases, and the resulting model was used to refine against the other data sets. Ligands were directly constructed into the corresponding difference electron density in each structure. Water molecules were included after the ligands were added.

The structure of *Pf*PurP in the small unit cell of space group *R*32 was determined by molecular replacement using the program MOLREP (31). A protomer of *Mj*PurP was used as the search model. The initial rigid body refinement and restrained refinement with the molecular replacement solution resulted in an *R* factor of 35%. The structures were further refined using the same procedure as described above for *Mj*PurP, and the refined model was used to determine the structures of *Pf*PurP in the other two crystal forms by molecular replacement. Model refinement statistics for the *Mj*PurP and *Pf*PurP structures are summarized in Table 2. The graphic figures of the structures were prepared using PyMOL (32).

## RESULTS

**Overview of *Mj*PurP and *Pf*PurP Structures.** The crystal structure of *Mj*PurP is a homohexamer (Figure 1A,B), consistent with the molecular weight analysis using size exclusion gel filtration. *Pf*PurP appeared to be predominantly trimeric in solution; however, *Pf*PurP in all three crystal forms showed a common hexameric arrangement (Figure 1C,D). While the trimeric substructures of *Mj*PurP and *Pf*PurP are nearly identical, the hexamers are slightly different. *Mj*PurP has ~2.5 times more buried surface area between the two trimers than *Pf*PurP (Table 3), resulting in an overall more compact structure. On the basis of the trimer superposition of the two structures, the same compact hexameric structure can be constructed for *Pf*PurP without causing significant close contacts, by rotating one trimer approximately 30° and translating it toward the opposing trimer.

**PurP Protomeric Fold.** *Mj*PurP and *Pf*PurP belong to the ATP grasp superfamily. Similar to that of other superfamily members, the molecular architecture of *Mj*PurP and *Pf*PurP consists of three motifs: the A, B, and C domains (Figure 2). Domain A is formed by residues 1–137/1–113 (the numbers correspond to *Mj*PurP/*Pf*PurP throughout). The core of domain A adopts a truncated Rossman fold, with a central four-stranded parallel β-sheet (3<sub>1</sub>2<sub>1</sub>1<sub>1</sub>4<sub>1</sub>) flanked by three α-helices. The structure of *Mj*PurP has two additional flanking helices (N-terminal α-helix H1a and 3<sub>10</sub>-helix H3a; helices present in only one of the PurP structures are



Table 2: Refinement Statistics

protein	<i>Mj</i> PurP	<i>Mj</i> PurP	<i>Mj</i> PurP	<i>Mj</i> PurP	<i>Pf</i> PurP	<i>Pf</i> PurP	<i>Pf</i> PurP	<i>Pf</i> PurP
complex	AICAR—AMPPCP	AICAR—ATP	FAICAR—ADP	AMP—AMP	AICAR—AMP	AMP—AMP	P <sub>i</sub> —ATP	P <sub>i</sub> —ADP
PDB code	2R7K	2R7L	2R7N	2R7M	2R84	2R85	2R86	2R87
space group	<i>R</i> 32	<i>R</i> 32	<i>R</i> 32	<i>R</i> 32	<i>R</i> 32	<i>R</i> 32	<i>R</i> 32	<i>P</i> 2 <sub>1</sub>
resolution (Å)	2.1	2.1	2.4	2.3	1.9	1.7	2.5	2.3
total no. of atoms	3035	3015	2942	2976	6308	6576	5535	17 028
no. of water atoms	108	128	58	94	624	656	133	541
<i>R</i> factor <sup>a</sup> (%)	20.8	20.9	21.2	20.4	17.5	16.6	21.9	20.3
<i>R</i> <sub>free</sub> <sup>b</sup> (%)	24.8	26.0	28.0	25.7	19.5	18.6	23.9	24.4
rmsd from ideal geometry								
bonds (Å)	0.006	0.006	0.007	0.007	0.007	0.008	0.007	0.007
angles (deg)	1.018	1.004	1.125	1.093	1.072	1.140	1.024	1.067
Ramachandran plot (%)								
most favored regions	91.0	92.0	89.1	91.3	91.1	90.6	90.7	89.1
additional allowed regions	8.7	7.7	10.3	8.4	8.6	9.1	8.7	10.3
generously allowed regions	0	0	0.3	0	0	0	0.3	0.3
disallowed regions <sup>c</sup>	0.3	0.3	0.3	0.3	0.3	0.3	0.3	0.3
av <i>B</i> factor (Å <sup>2</sup> )	48.1	44.1	51.3	46.2	21.8	17.5	47.9	22.3

<sup>a</sup> *R* factor =  $\sum_{hkl} ||F_o| - k|F_c|| / \sum_{hkl} |F_o|$ , where  $F_o$  and  $F_c$  are observed and calculated structure factors, respectively. <sup>b</sup> For  $R_{free}$  the sum is extended over a subset of reflections (5%) excluded from all stages of refinement. <sup>c</sup> The residue in the disallowed region of the Ramachandran plot corresponds to His27 for *Mj*PurP and His11 for *Pf*PurP.

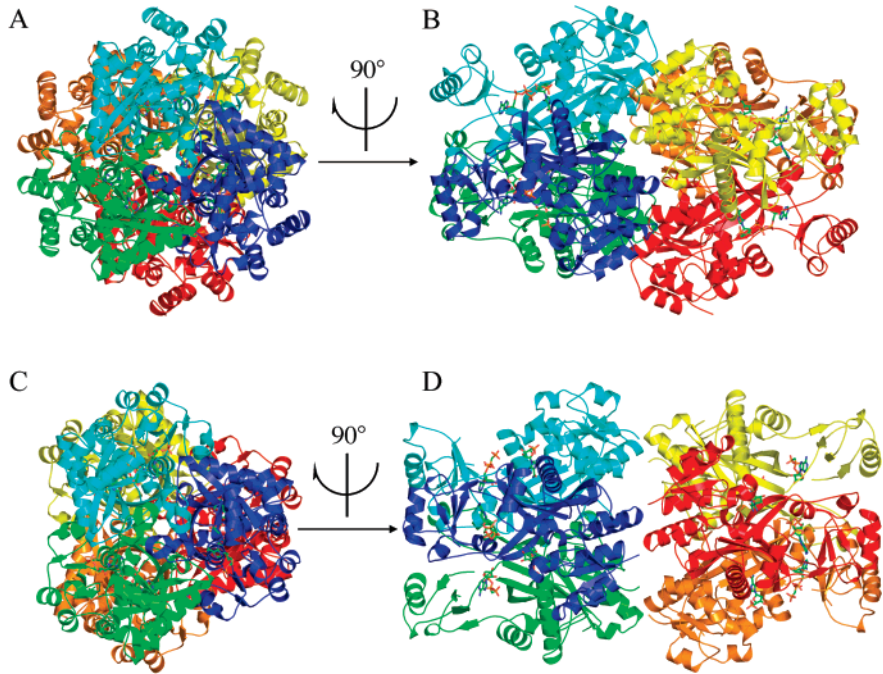


FIGURE 1: Structures of *Mj*PurP and *Pf*PurP. The hexameric crystal structures of *Mj*PurP (A, B) and *Pf*PurP (C, D) are shown in ribbon diagrams and colored by protomer. Compared to that of *Mj*PurP, the hexameric arrangement of *Pf*PurP has significantly less interactions at the trimer—trimer interface and is possibly a crystallization artifact rather than biologically relevant.

Table 3: Buried Surface Area (Å<sup>2</sup>)

interface	<i>Mj</i> PurP	<i>Pf</i> PurP
3-fold (subunit A—B)	4100	4100
2-fold (trimer—trimer)	4600	1800

designated H). In addition to the core, the last 40 amino acids of domain A contain four more helices:  $\alpha$ 4,  $\alpha$ 5, H6a ( $\alpha$ -helix in *Mj*PurP and  $3_{10}$ -helix in *Pf*PurP), and  $\alpha$ 6. Helices  $\alpha$ 4 and  $\alpha$ 5 pack against the core motif, while H6a and  $\alpha$ 6 wrap around domain C and serve as a linker between domain A and domain B. Domain B is the smallest domain of the three, consisting of residues 138–204/114–180. The structure of domain B is an  $\alpha\beta$  two-layered sandwich, comprised of a four-stranded antiparallel  $\beta$ -sheet ( $5\uparrow 8\downarrow 6\uparrow 7\downarrow$ ) and three flanking helices on the solvent-exposed face:  $3_{10}1$ ,  $\alpha$ 7, and H7a ( $\alpha$ -helix in *Mj*PurP and  $3_{10}$ -helix in *Pf*PurP). Domain

C is composed of residues 205–361/179–334. The core of domain C is a twisted  $\beta$ -sheet consisting of five antiparallel strands ( $13\downarrow 12\uparrow 9\downarrow 10\uparrow 11\downarrow$ ) and flanked by a long helix,  $\alpha$ 9, on one side and four helices on the other side,  $3_{10}2$ , H10a ( $\alpha$ -helix in *Mj*PurP and  $3_{10}$ -helix in *Pf*PurP),  $\alpha$ 10, and  $3_{10}3$ . Two helices, H8a ( $\alpha$ -helix in *Mj*PurP and  $3_{10}$ -helix in *Pf*PurP) and  $\alpha$ 8, extend away from the core motif. These two helices and strands  $\beta$ 10 and  $\beta$ 11 contribute significantly to the subunit interface by interacting with the same region from the two adjacent protomers related by the 3-fold crystallographic symmetry.

**Active Site Cleft.** The assembly of the A, B, and C domains forms an active site cleft of approximately  $25 \text{ Å} \times 15 \text{ Å} \times 10 \text{ Å}$ , with the long  $\beta$ -sheet from the C domain as the bottom. The AICAR/FAICAR binding pocket is formed between domains A and C and a small part of domain C from an

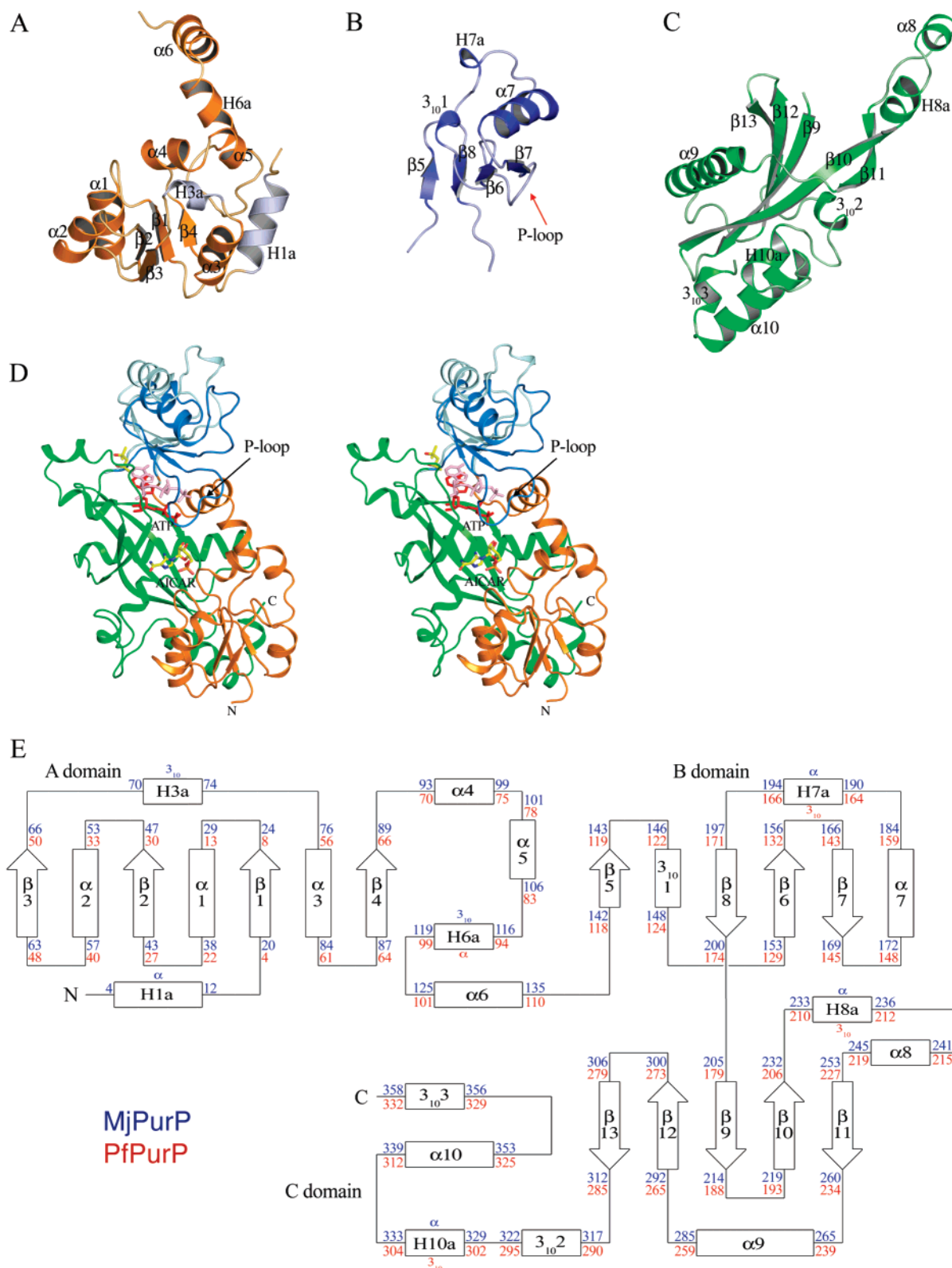


FIGURE 2: Conserved protomer architecture of *MjPurP* and *PfPurP*. (A) A domain. The two insertion helices of *MjPurP* are colored in light blue. (B) B domain. (C) C domain. (D) Stereodivision of the protomer colored by domain. The B domain in closed and open conformations is in dark blue and light blue, respectively, and the corresponding ADP/ATP in red and pink, respectively. (E) Topology diagram. The conserved secondary structural elements between *MjPurP* and *PfPurP* are numbered consecutively. The residue numbers are indicated in blue for *MjPurP* and red for *PfPurP*.

adjacent protomer. The secondary structural elements involved in the AICAR/FAICAR binding site include  $\alpha 4$ ,  $\beta 11$ ,  $\alpha 9^*$ , and loops connecting  $\beta 1$  and  $\alpha 1$ ,  $\beta 2$  and  $\alpha 2$ , and  $\beta 11^*$  and  $\alpha 9^*$  (the asterisk indicates a symmetry-related protomer

throughout). The ATP binding site is sandwiched between the  $\beta$ -sheets from the B domain ( $\beta 6$ ,  $\beta 7$ , and  $\beta 8$ ) and C domain ( $\beta 10$ ,  $\beta 12$ , and  $\beta 13$ ). Helix H8a\* and the loop region following it also contribute to the ATP binding site.

**Domain Movement Observed for Domain B.** Two main conformations were observed in the structures of *MjPurP* and *PfPurP*: a closed conformation for all *MjPurP* structures and the  $P_i$ -ADP complex of *PfPurP* and an open conformation for the rest of the *PfPurP* structures. In the closed conformation, the ATP binding site and the AICAR/FAICAR binding site are close together, while in the open conformation the two sites are farther apart (Figure 2D). Loop 136–141/111–117 and loop 201–204/175–178 appear to serve as hinges, allowing the B domain to move and consequently to open and close over the substrate binding site.

**P-Loop.** The structures of *MjPurP* complexed with AICAR-ATP and with AICAR-AMPPCP (the nomenclature follows ligands bound at the AICAR/FAICAR site and the ATP site, separated by an en dash) have clear density for the nucleotide triphosphate molecule, indicating that the ligand is relatively well ordered and fully occupied in the active site. In contrast, the predicted P-loop for ATP binding is partially disordered. Among all the *MjPurP* structures, the AICAR-AMPPCP complexed structure shows the most complete P-loop with only three residues missing (161 RGG 163). For *PfPurP*, the complete polypeptide chain was built for the  $P_i$ -ADP complex (space group  $P2_1$ ) and subunit A of the  $P_i$ -ATP complex (space group  $R32$ , large unit cell). However, the P-loop (135 GAKGG 139) and the  $\beta$ - and  $\gamma$ -phosphates exhibit relatively high temperature factors and weaker electron densities, suggesting significant flexibility. The structures of *PfPurP* crystallized in the small unit cell of space group  $R32$  were determined at higher resolution (1.7–1.9 Å); however, the electron density is only interpretable for the AMP moiety even though ATP or AMPPCP was present in the crystallization condition. Consistent with the disordered phosphate groups, residues 134–140 from the P-loop also lack interpretable electron density and were omitted from the final model in this crystal form of *PfPurP*.

**AICAR/FAICAR Binding Site of *MjPurP*.** We have determined the structures of *MjPurP* in four different ligand complexes: AICAR-ATP, AICAR-AMPPCP, FAICAR-ADP, and AMP-AMP. The substrate AICAR binds essentially the same in the AICAR-ATP and the AICAR-AMPPCP complex structures. The ribose moiety of the AICAR molecule is in a slightly twisted 3'-endo conformation (Figure 3A). Surprisingly, the ribose hydroxyl groups are solvent exposed and lack hydrogen bond interaction with any active site residues (Figure 3B). The aminoimidazole-carboxamide moiety is mostly anchored through a pair of hydrogen bonds between the carboxamide and the Asn258 side chain. His27, Ile255, Asp316, and Gly317 also help to orient the imidazole ring through van der Waals interactions. In addition, a water molecule that hydrogen bonds to the carbonyl oxygen of His27 and the backbone amide of Glu265\* also hydrogen bonds to the imidazole. A chloride anion, presumably an artifact due to the high concentration of NaCl in the crystallization condition, was modeled near the AICAR imidazole ring on the basis of the intensity of the electron density and the positively charged binding environment: His27 and Arg314 interact with the chloride anion through electrostatic interactions/hydrogen bonds (Figure 3A). The 5'-monophosphate is positioned by a total of six hydrogen bond interactions. Ser94 and Ser266\* each provide a hydrogen bond to the phosphate with the side chain hydroxyl group, the guanidinium group of Arg264\* donates

two hydrogen bonds, and the last two hydrogen bonds are provided by water molecules, which in turn hydrogen bond to the Arg51 side chain and the backbone amide of Ser266\*.

In the structure of *MjPurP* complexed with the products FAICAR and ADP, the binding geometry of FAICAR is similar to that of AICAR, except that the ribose moiety of FAICAR is in a slightly twisted 4'-endo conformation (Figure 3C,D). The substrate binding site residues superimpose well between the two structures. The most significant differences are for Arg314: the C $\alpha$  position moves approximately 0.5 Å closer to the ligand upon FAICAR binding. The guanidinium group of Arg314 is in the vicinity of the formyl group of FAICAR and donates a hydrogen bond with a distance of 2.9 Å. However, Arg314 has weak density for the guanidinium group in the FAICAR-ADP complex structure, which suggests high thermal motion. This thermal motion is probably related to the FAICAR binding, since Arg314 has clear electron density and a relatively low temperature factor in the AICAR-ATP structure. The relatively weak density for the formyl group carbon atom suggests that the formyl group also undergoes some thermal motion. Besides Arg314, the His27 side chain and the backbone amide of Gly317 are also potential hydrogen bond donors to the formyl group.

In the structure of the *MjPurP* complex with AMP, one AMP molecule is bound in the AICAR/FAICAR binding site and the second AMP is bound in the ATP binding site. The binding geometry of AMP at the AICAR/FAICAR binding site is essentially the same as that of AICAR, except that the Asn258 side chain is flipped to form hydrogen bonds with both the N1 atom and the N6 amine of the adenine base.

**ATP Binding Site of *MjPurP*.** While the AICAR molecule is somewhat solvent exposed, the ATP molecule is mostly buried within the active site (Figure 3E,F). The ATP binding environment can be divided into three components: the base binding site, the ribose binding site, and the triphosphate binding site. The adenine base is oriented through a mixture of hydrophobic interactions and hydrogen bonds. Ile154 and Tyr201 pack against the adenine base from one side, while Leu299 and Phe309 pack on the other side. There are a total of four hydrogen bonds between the base and the enzyme. The N1 atom forms a hydrogen bond to the backbone amide of Val202. The N6 amino group donates two hydrogen bonds to the Glu199 side chain carboxylate and the carbonyl group of Glu200. The N7 atom accepts a hydrogen bond from Lys156. The ribose moiety is in the 3'-endo conformation, and the hydroxyl groups of the ribose form a total of three hydrogen bonds to Glu230 and Arg238\*. In addition, Tyr253 and Phe309 stack against the hydrophobic faces of the ribose. The  $\alpha$ -phosphate accepts two hydrogen bonds from Lys156 and Tyr166, and the  $\beta$ -phosphate forms one hydrogen bond with the carboxamide of Gln297. The  $\gamma$ -phosphate does not form any direct hydrogen bond with the protein; however, the  $\gamma$ -phosphate forms two hydrogen bonds with the AICAR molecule (Figure 3B). In addition, water molecules are found to bridge between the  $\gamma$ -phosphate and active site residues, including Arg228, Tyr253, and Gln297 (Figure 3E).

The nonhydrolyzable ATP analogue AMPPCP binds at the active site in a geometry similar to that for ATP, with the only difference coming from the positioning of the  $\gamma$ -phosphate. The  $\gamma$ -phosphate of AMPPCP binds more



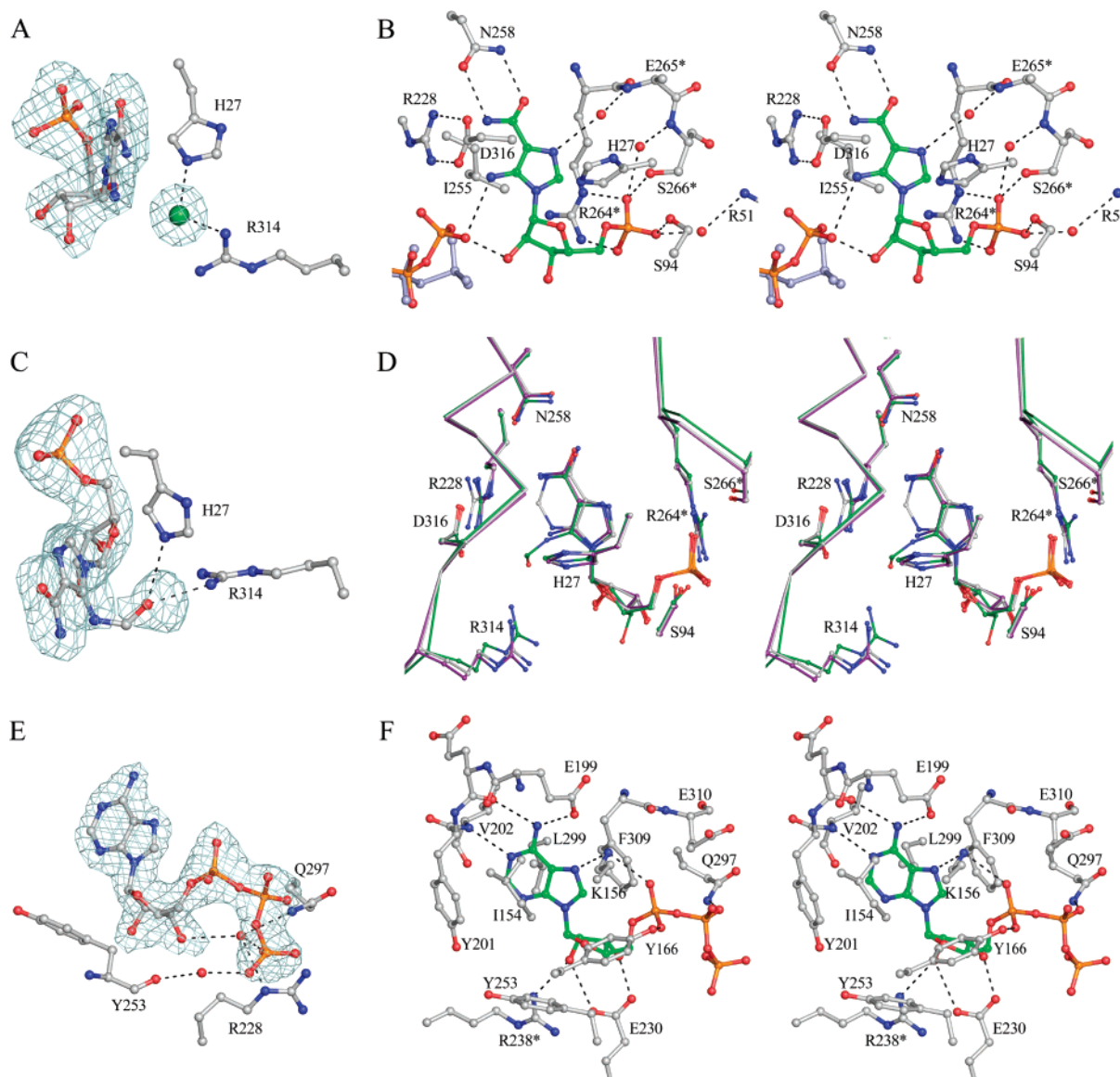


FIGURE 3: Active site of *MjPurP*. (A)  $F_o - F_c$  density contoured at  $3\sigma$  around AICAR and the chloride anion (green) of the AICAR–ATP structure. (B) Stereodiagram of the AICAR binding site for the AICAR–ATP structure. The  $\gamma$ -phosphate of AMPPCP from the AICAR–AMPPCP structure is superimposed and colored in light blue. Hydrogen bonds are indicated by dashed lines. (C)  $F_o - F_c$  density contoured at  $3\sigma$  around FAICAR of the FAICAR–ADP structure. (D) Superposition of AICAR (purple), FAICAR (green), and AMP (gray) at the active site. (E)  $F_o - F_c$  density contoured at  $3.5\sigma$  around ATP of the AICAR–ATP structure. (F) Stereodiagram of the ATP binding site.

toward the solvent and makes only one hydrogen bond to the 2'-hydroxyl group of AICAR (Figure 3B). Although  $Mg^{2+}$  ions were present in the crystallization and soaking solutions, there is no evidence of  $Mg^{+2}$  binding in any of the *MjPurP* structures.

**AICAR Binding Site of *PfPurP*.** The AICAR molecule was modeled in two conformations that differ mostly in the conformation of the ribose moiety: the 3'-*endo* and 2'-*endo* sugar conformations represent approximately 70% and 30% of the occupancy, respectively. Despite the conformational difference, the two conformers bind to the enzyme through similar interactions. Given only four residues being different (Tyr98/His75, Ile255/Val229, Asp316/Val289, and Gly317/Ala290, corresponding to *MjPurP*/*PfPurP* throughout), the AICAR binding scheme is remarkably similar to that of *MjPurP*, with most interactions through the aminoimidazole-carboxamide moiety and the 5'-monophosphate (Figures 4A,B and 5A). His75 and Ser10, whose structural equivalents

Tyr98 and Ser26 in *MjPurP* are positioned too far for hydrogen-bonding interactions, provide two additional hydrogen bonds to the 5'-monophosphate. As is the case for the structure of *MjPurP*, a chloride anion is also found near the AICAR molecule, forming salt bridges or hydrogen bonds with His11 and Arg287.

In the  $P_i$ -ATP and  $P_i$ -ADP structures of *PfPurP*, inorganic phosphates, presumably coming from the crystallization conditions, are bound at both the AICAR binding site and the chloride binding site. The overlay of the structures showed that the second phosphate group has an oxygen atom superimposed with the chloride and forms a total of five hydrogen bonds with His11, Arg202, Arg287, and the main chain amide of Ala290 (Figure 4D). In the AMP–AMP structure of *PfPurP*, the monophosphate nucleotide is bound at the AICAR binding site as well as the ATP binding site; however, in the AICAR binding site the orientation of the AMP is flipped relative to the substrate. Besides the

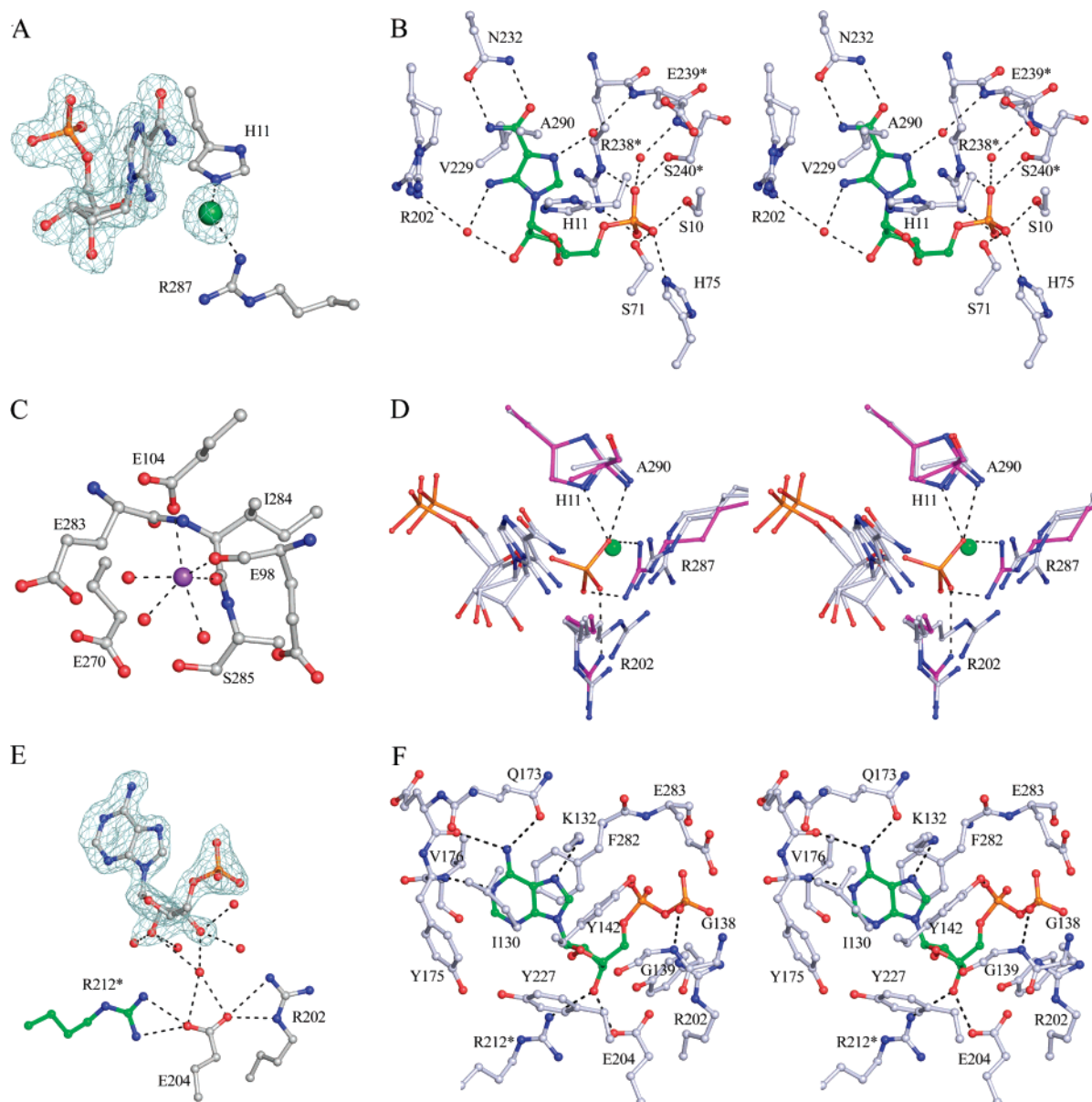


FIGURE 4: Active site of *PfPurP*. (A)  $F_o - F_c$  density contoured at  $3.5\sigma$  around AICAR and the chloride anion. For clarity only the 3'-endo conformer of AICAR is shown. (B) Stereodigram of the AICAR binding site. Arg202 is built in alternate conformations. (C) Putative sodium ion (purple) binding site. The binding of the sodium ion is presumably a crystallization artifact. (D) AICAR binding sites of the AICAR-AMP structure (silver blue) and  $P_i$ -ATP structure (magenta) superimposed. The phosphate oxygen from the  $P_i$ -ATP structure overlies the chloride atom from the AICAR-AMP structure. (E) AMP bound at the ATP binding site in the open conformation, with  $F_o - F_c$  density contoured at  $3.5\sigma$ . (F) Stereodigram of the ATP binding site of the  $P_i$ -ADP structure in the closed conformation.

interactions with the 5'-monophosphate, an additional hydrogen bond is formed between the N6 amino group and the carbonyl group of Ala74. The binding of the AMP molecule at the AICAR binding site is only observed at high concentration of the nucleotide (50 mM) and is probably not biochemically relevant.

**ATP Binding Site of *PfPurP*.** The  $P_i$ -ADP complex structure in space group  $P2_1$  is the only *PfPurP* structure in the closed conformation. In this conformation the ADP molecule forms two hydrogen bonds through the 3'-hydroxyl group to Glu204 and Arg212\*. The 2'-hydroxyl group forms a hydrogen bond to a water molecule that in turn hydrogen bonds to the carbonyl group of Gly271. The P-loop encircles the  $\beta$ -phosphate and forms a hydrogen bond through Gly139. The rest of the ATP binding interactions resemble that of *MjPurP* (Figures 4F and 5B), with only four residue

substitutions (Glu199/Gln173, Cys208/Tyr182, Gln297/Glu270, and Leu299/Val272).

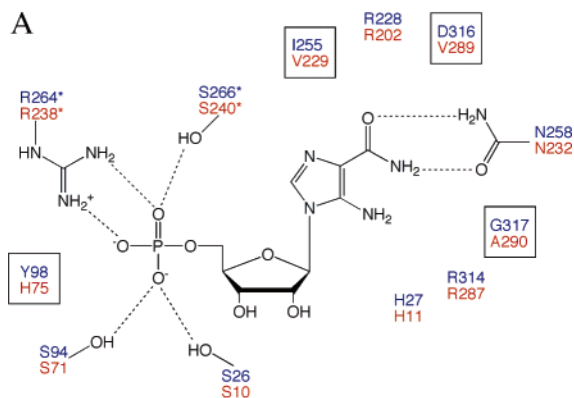
In the remaining *PfPurP* structures, which are all in the open conformation, the ribose moiety of ATP does not make any direct hydrogen bond interactions to the enzyme; however, a water molecule was found to bridge between Glu204 and the hydroxyl group of the ribose (Figure 4E).

A metal ion was observed between the ATP binding site and the AICAR binding site for the structures of *PfPurP* in the open conformation, coordinated by the carboxylate group of Glu104, the carbonyl groups of Glu98 and Ile284, and three water molecules in an octahedral geometry (Figure 4C). The coordination bond distances range from 2.3 to 2.6 Å. On the basis of the binding geometry and the size of the electron density, a sodium atom that presumably came from the crystallization buffer was modeled at the metal binding



MjPurP  
PfPurP

A



B

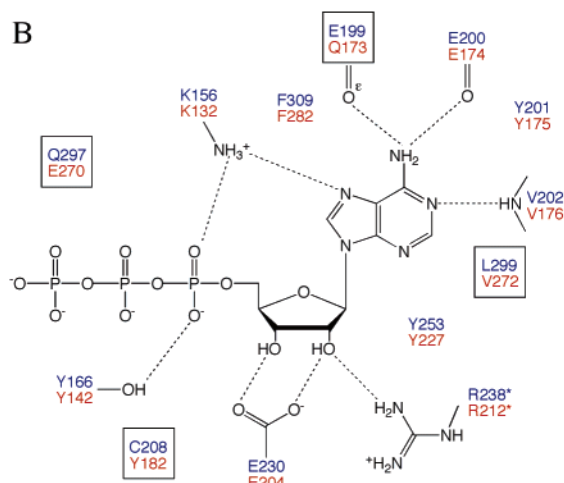


FIGURE 5: Active site comparison of *MjPurP* and *PfPurP*. The active site residues are indicated in blue for *MjPurP* and red for *PfPurP*. In the AICAR binding site (A), only four residues are different between the two structures and are highlighted by boxes: Tyr98/His75, Ile255/Val229, Asp316/Val289, and Gly317/Ala290 (corresponding to *MjPurP*/*PfPurP* throughout). In the ATP binding site (B), also only four residues are different and are highlighted: Glu199/Gln173, Cys208/Tyr182, Gln297/Glu270, and Leu299/Val272.

site; however, the density might also represent a partially occupied magnesium ion.

## DISCUSSION

**Structural Comparison of PurP with Other ATP Grasp Superfamily Members.** Many ATP grasp superfamily members have been structurally characterized, including glycylamide ribonucleotide synthetase (PurD) (21), phosphoribosylglycinamide transformylase (PurT) (14), *N*<sup>5</sup>-carboxyaminoimidazole ribonucleotide synthetase (PurK) (22), phosphoribosylaminoimidazolesuccinocarboxamide synthetase (PurC) (23, 24), biotin carboxylase (20), carbamoyl phosphate synthetase (33–35), D-Ala-D-Ala ligase (36), and glutathione synthetase (37, 38). Interestingly, PurD, PurT, PurK, PurC, and PurP all belong to the purine biosynthetic pathway. Using the structure of *MjPurP* as the reference, a structural homology search and comparison was performed with DALI (39), and the results are summarized in Table 4. PurD, PurT, PurK, and PurP are more structurally similar to each other, while PurC only shares a similar topology with

Table 4: DALI Search and Structure Comparison (39) Using the Structure of *M. jannaschii* PurP (2R7K) as the Reference<sup>a</sup>

structure	PDB ID	Z <sup>b</sup>	rmsd <sup>c</sup>	no. of aligned residues	identity (%)
<i>PfPurP</i> (closed)	2R87	42.3	1.4	322	50
<i>PfPurP</i> (open)	2R84	40.0	2.2	319	50
<i>TkPurP</i> (unknown function)	2PBZ	34.9	1.7	287	36
PurD	1GSO	19.8	3.5	282	11
PurT	1EZ1	19.5	3.7	269	14
carbamoyl phosphate synthetase	1KEE	18.4	4.1	270	16
biotin carboxylase	1BNC	17.9	5.2	270	15
PurK	1B6R	17.1	3.1	244	11
D-Ala-D-Ala ligase	1IOW	14.4	3.8	250	14
glutathione synthetase	1GSA	14.3	3.5	247	13
lysine biosynthesis enzyme	1UC8	13.9	3.2	226	12
Lysx					
synapsin Ia fragment	1AUV	13.3	3.5	236	11
inositol 1,3,4-trisphosphate 5/6 kinase	1Z2N	12.5	3.9	232	10

<sup>a</sup> Structures of hypothetical proteins or a Z score below 10.0 are not included. <sup>b</sup> Z = strength of structural similarity in standard deviations above the expected. <sup>c</sup> rmsd = root mean square deviation.

the C domain, although PurD, PurT, and PurK have an additional C-terminal domain of approximately 70 residues compared to PurP.

ATP or ADP complex structures have been determined for all ATP grasp members from the purine biosynthetic pathway except for PurD; however, an ordered P-loop has only been observed for PurT, PurC, and *PfPurP*. Despite the low sequence conservation among the five enzymes, structural alignment of PurC, PurD, PurK, PurT, and PurP revealed significant similarities at the ATP binding site shown in Figure 6. Because Mg<sup>+2</sup> was present in the crystallization solutions and is required for activity, it is surprising that no Mg<sup>+2</sup> ions were found in the active site of PurP. This may be a crystallization artifact caused by the interference of high salt concentrations. On the basis of the structural comparison with other ATP grasp members, Glu310 of *MjPurP* is probably involved in Mg<sup>+2</sup> binding in solution (Figure 6).

PurD, PurT, PurK, PurC, and PurP all recognize 5'-monophosphate substrates specifically. Structures of PurP, PurT, and PurC complexed with a 5'-monophosphate ligand are available. While the 5'-monophosphate ligands are generally in the same part of the fold, the details of binding are different for the four structures, which presumably have evolved to accommodate their specific substrates.

**Domain B and Substrate Binding Site Closure.** The open and closed conformations observed in the structures of *PfPurP* suggest that a hingelike movement of domain B is associated with active site closure. In both conformations an ATP or ADP molecule is bound at the active site; however, an MPD molecule identified on the domain interface of domains B and C, which is presumably a structural artifact, may help stabilize the open conformation (Figure 2D). Similar conformational changes in the B domain between the unliganded and ATP-bound structures have been observed for PurK (22), carbamoyl phosphate synthetase (33–35), and glutathione synthetase (37, 38). These observations suggest that B domain closure is probably a common feature of the ATP grasp superfamily and is associated with ATP binding.

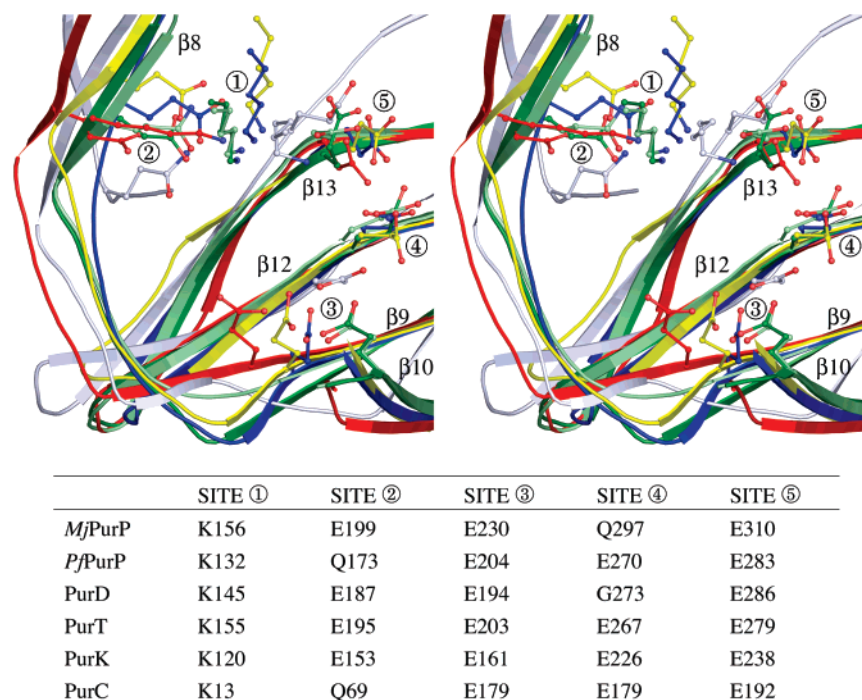
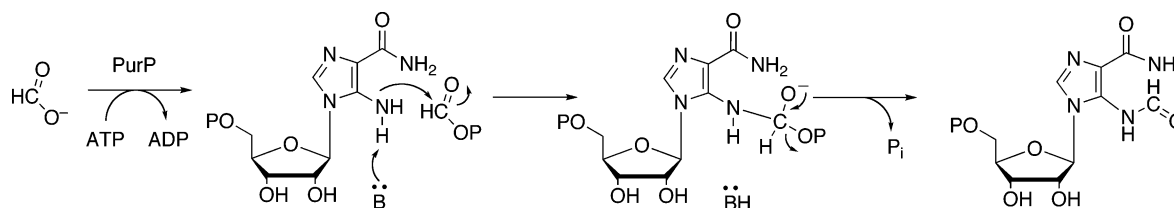


FIGURE 6: Superposition of the ATP binding motif of PurD (1GSO, red), PurT (1EZ1, blue), PurK (1B6S, yellow), PurC (2GQS, silver blue), *MjPurP* (dark green), and *PfPurP* (light green). For site 1, a structurally conserved lysine residue from the P-loop is associated with  $\alpha$ -phosphate binding. For site 2, a glutamate or glutamine residue is responsible of base binding through a hydrogen bond to the N6 amine. This conserved glutamate or glutamine resides on  $\beta$ 8 (using the nomenclature of PurP's) except for PurC, in which case the glutamine comes from an adjacent  $\beta$ -strand. For site 3, a glutamate residue, however coming from different  $\beta$ -strands ( $\beta$ 10 for *MjPurP* and *PfPurP*,  $\beta$ 9 for PurD, PurT, and PurK, and  $\beta$ 12 for PurC), forms or potentially can form hydrogen bonds to the hydroxyl groups of the ribose. Sites 4 and 5 are involved in  $Mg^{+2}$  binding in the structures of PurT and PurK.

#### Scheme 1



**Mechanistic Implications.** PurP catalyzes an ATP-dependent ligation and is structurally and functionally unrelated to the bifunctional enzyme PurH (9). As is characteristic of ATP grasp enzymes, the substrate of PurP is activated by ATP-dependent phosphorylation. A formyl phosphate intermediate is predicted, as is the case for *E. coli* PurT (13) (Scheme 1). The reaction would also be mechanistically analogous to the formylglycinamide ribonucleotide (FGAR) amidotransferase (PurL) reactions (40, 41) involved in the conversion of FGAR to formylglycinamide ribonucleotide (FGAM) and the aminoimidazole ribonucleotide (AIR) synthetase (PurM) reaction converting FGAM to AIR (21, 42). Both of these enzymes are believed to utilize iminophosphate intermediates. The PurM and PurL enzymes belong to a different superfamily of enzymes than ATP grasp.

Attempts to crystallize the PurP–AICAR–formate–AMPPCP complex were unsuccessful; however, the *MjPurP*–AICAR–AMPPCP complex binds chloride anion, which likely occupies the formyl phosphate or formate binding site and prevents formate from binding. The *PfPurP*–AICAR–AMP complex also showed a chloride in the same position as the chloride in *MjPurP*; however, in both the *PfPurP*– $P_i$ –ADP and *PfPurP*– $P_i$ –ATP complexes, a phosphate occupies the chloride binding site. Modeling studies based

on these observations, in which a formyl phosphate intermediate is positioned in the chloride binding site, show good active site geometry (Figure 7). The FAICAR synthetase reaction requires a base near the 5-amino group of AICAR. His27 of *MjPurP*, which is conserved throughout all PurP sequences, possibly provides this function.

**Sequence Analysis of PurP-like Genes.** PurP is found in most Archaea with more than one copy. *P. furiosus*, for example, has two *purP* genes (Pf0421 and Pf1517). In preliminary studies, neither *P. furiosus* gene product showed detectable FAICAR synthetase activity. This observation raises the possibility that the duplicated genes might have alternative functions. To explore this possibility, we performed a phylogenetic analysis of PurP sequences. Using *MjPurP* as the search sequence, a BLAST search (43) revealed 41 putative PurP sequences after removal of duplicates and partial sequences. These sequences come from a total of 22 archaeal organisms, 17 of which contain either two or three *purP* genes, and share approximately 30–90% sequence identity. A sequence alignment and phylogenetic tree (Figure 8) were generated using CLUSTALW (44). The *purP* genes divide into three groups with two outliers. The first group has five members: *M. jannaschii*, *Methanococcus maripaludis*, *Methanopyrus kandleri*, *Methanosphaera stadt-*

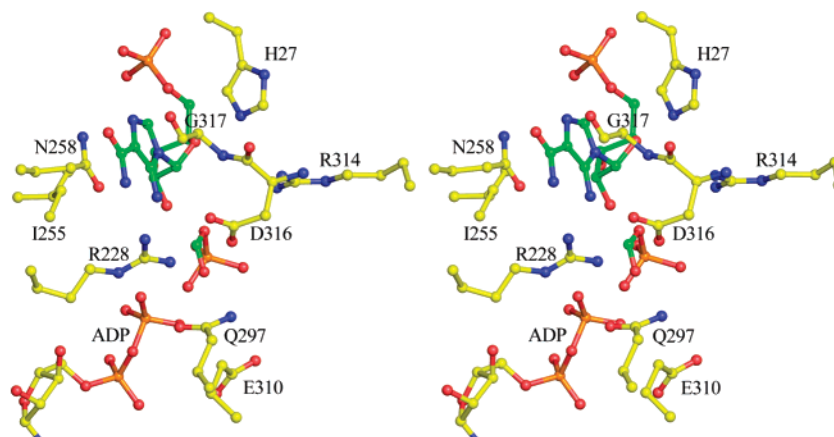


FIGURE 7: Modeled formyl phosphate intermediate for the FAICAR synthetase reaction at the *MjPurP* active site. The intermediates were modeled to optimize the reaction trajectories while using the observed AICAR/FAICAR binding sites as a constraint.

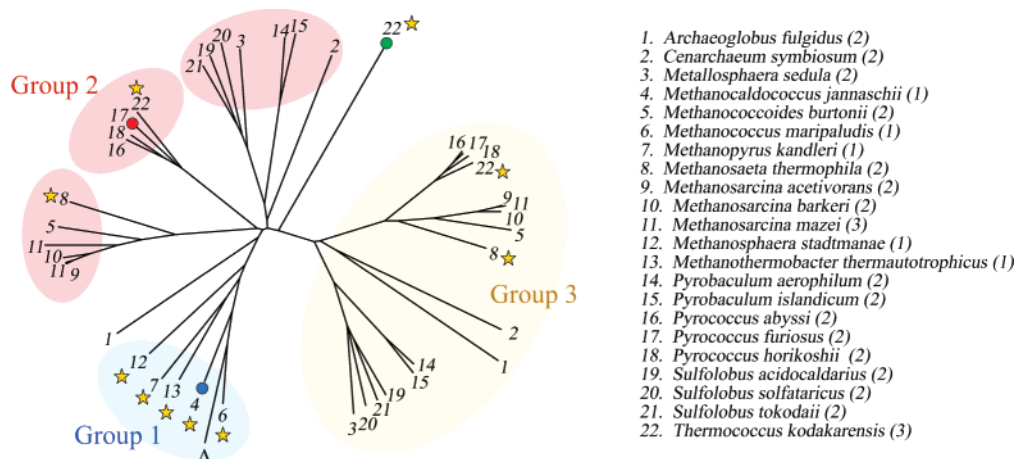


FIGURE 8: Phylogenetic analysis of PurP orthologues. The species containing PurP-like sequences are numbered in alphabetical order, with the number of PurP alternate forms listed in parentheses. *MjPurP*, *PfPurP*, and PDB structure 2PBZ are highlighted by blue, red, and green circles, respectively. The *purO* gene containing species are indicated by stars. The symbol  $\Delta$  indicates a partial PurP sequence from *Methanococcus vannielii*, whose complete genome is not available at this point.

*manae*, and *Methanothermobacter thermautotrophicus*. They each contain a single *purP* gene, and we conclude that these five PurP's are FAICAR synthetases. Fifteen organisms, including *P. furiosus*, have two *purP* genes with one group 2 PurP and one group 3 PurP. *PfPurP* (Pf1517) belongs to group 2, which can be further divided into three subgroups, and the second *P. furiosus* PurP (Pf0421) belongs to group 3. No gene product from group 2 or group 3 has been functionally characterized. One of the PurP's from *Thermococcus kodakarensis*, which represents an outlier from the alignment, has recently been structurally characterized with ATP bound at the active site (PDB 2PBZ) by the New York Structural GenomiX Research Consortium (NYSGXRC). Structure 2PBZ shares approximately 30% sequence identity to both *MjPurP* and *PfPurP* and forms a trimer.

Further analysis of the sequence alignment revealed that key active site residues are mostly conserved for group 1 and 2 members but not for group 3. Asn258/232, the asparagine residue interacting with the carboxamide of AICAR, is conserved for groups 1 and 2 but replaced by a histidine residue in all the group 3 sequences. In addition, the motif KX<sub>6</sub>GR(K)G present in groups 1 and 2 corresponding to the P-loop is replaced by KX<sub>8</sub>ERG(A) at the aligned position for group 3. These observations raise the questions of (1) whether group 2 members also function as

FAICAR synthetases, but perhaps utilizing a different formyl source, and (2) whether group 3 members are silent genes, catalyze a different reaction, or have other noncatalytic functions.

Additional questions remain to be answered regarding the identification of the enzymes that catalyze the last two steps of purine biosynthesis in Archaea. PurO, the known IMP cyclohydrolase for the final step, is not commonly present in Archaea. With the exception of *Methanosaeta thermophila* and *T. kodakarensis*, the *purO* gene is found only in the five species with a single *purP* gene (group 1) and four halobacteria organisms where the *purP* gene is missing altogether. Therefore, PurO probably functions as an uncommon catalyst for the last step of purine biosynthesis. *MjPurP* is the only enzyme with confirmed AICAR transformylase activity in Archaea to date. As a signature gene PurP's are widely present in Archaea, and given the high sequence homology among the PurP groups, it is tempting to speculate that group 2 PurP's are responsible for FAICAR synthetase activity or might even catalyze the ATP-dependent ring closure to form IMP. However, it is also possible that enzymes yet to be identified in Archaea catalyze these two reactions. The answer to these intriguing questions awaits further biochemical and structural investigations.



## ACKNOWLEDGMENT

We thank Leslie Kinsland for assistance in the preparation of the manuscript. We thank the NE-CAT staff at beamline 24-ID-C of the Advanced Photon Source and MacCHESS for assistance with data collection.

## REFERENCES

- Buchanan, J. M., and Hartman, S. C. (1959) Enzymatic reactions in the synthesis of purines, *Adv. Enzymol.* 21, 199–261.
- Mueller, E. J., Meyer, E., Rudolph, J., Davisson, V. J., and Stubbe, J. (1994) *N*<sup>5</sup>-carboxyaminoimidazole ribonucleotide: evidence for a new intermediate and two new enzymatic activities in the *de novo* purine biosynthetic pathway of *Escherichia coli*, *Biochemistry* 33, 2269–2278.
- Meyer, E., Leonard, N. J., Bhat, B., Stubbe, J., and Smith, J. M. (1992) Purification and characterization of the *purE*, *purK*, and *purC* gene products: Identification of a previously unrecognized energy requirement in the purine biosynthetic pathway, *Biochemistry* 31, 5022–5032.
- Meyer, E., Kappock, T. J., Osuji, C., and Stubbe, J. (1999) Evidence for the direct transfer of the carboxylate of *N*<sup>5</sup>-carboxyaminoimidazole ribonucleotide (*N*<sup>5</sup>-CAIR) to generate 4-carboxy-5-aminoimidazole ribonucleotide catalyzed by *Escherichia coli* *PurE*, an *N*<sup>5</sup>-CAIR mutase, *Biochemistry* 38, 3012–3018.
- Aimi, J., Qiu, H., Williams, J., Zalkin, H., and Dixon, J. E. (1990) *De novo* purine nucleotide biosynthesis: cloning of human and avian cDNAs encoding the trifunctional glycinamide ribonucleotide synthetase-aminoimidazole ribonucleotide synthetase-glycinamide ribonucleotide transformylase by functional complementation in *E. coli*, *Nucleic Acids Res.* 18, 6665–6672.
- Firestone, S. M., and Davisson, V. J. (1994) Carboxylases in *de novo* purine biosynthesis. Characterization of the *Gallus gallus* bifunctional enzyme, *Biochemistry* 33, 11917–11926.
- Chen, Z. D., Dixon, J. E., and Zalkin, H. (1990) Cloning of a chicken liver cDNA encoding 5-aminoimidazole ribonucleotide carboxylase and 5-aminoimidazole-4-*N*-succinocarboxamide ribonucleotide synthetase by functional complementation of *Escherichia coli* *pur* mutants, *Proc. Natl. Acad. Sci. U.S.A.* 87, 3097–3101.
- Ni, L., Guan, K., Zalkin, H., and Dixon, J. E. (1991) *De novo* purine nucleotide biosynthesis: cloning, sequencing and expression of a chicken *PurH* cDNA encoding 5-aminoimidazole-4-carboxamide-ribonucleotide transformylase-IMP cyclohydrolase, *Gene* 106, 197–205.
- Greasley, S. E., Horton, P., Ramcharan, J., Beardsley, G. P., Benkovic, S. J., and Wilson, I. A. (2001) Crystal structure of a bifunctional transformylase and cyclohydrolase enzyme in purine biosynthesis, *Nat. Struct. Biol.* 8, 402–406.
- Rayl, E. A., Moroson, B. A., and Beardsley, G. P. (1996) The human *purH* gene product, 5-aminoimidazole-4-carboxamide ribonucleotide formyltransferase/IMP cyclohydrolase. Cloning, sequencing, expression, purification, kinetic analysis, and domain mapping, *J. Biol. Chem.* 271, 2225–2233.
- Wolan, D. W., Cheong, C. G., Greasley, S. E., and Wilson, I. A. (2004) Structural insights into the human and avian IMP cyclohydrolase mechanism via crystal structures with the bound XMP inhibitor, *Biochemistry* 43, 1171–1183.
- Marolewski, A., Smith, J. M., and Benkovic, S. J. (1994) Cloning and characterization of a new purine biosynthetic enzyme: a non-folate glycinamide ribonucleotide transformylase from *E. coli*, *Biochemistry* 33, 2531–2537.
- Marolewski, A. E., Mattia, K. M., Warren, M. S., and Benkovic, S. J. (1997) Formyl phosphate: a proposed intermediate in the reaction catalyzed by *Escherichia coli* *PurT* GAR transformylase, *Biochemistry* 36, 6709–6716.
- Thoden, J. B., Firestone, S., Nixon, A., Benkovic, S. J., and Holden, H. M. (2000) Molecular structure of *Escherichia coli* *PurT*-encoded glycinamide ribonucleotide transformylase, *Biochemistry* 39, 8791–8802.
- Owby, K., Xu, H., and White, R. (2005) A *Methanocaldococcus jannaschii* archeal signature gene encodes for a 5-formaminoimidazole-4-carboxamide-1- $\beta$ -D-ribofuranosyl 5'-monophosphate synthetase: A new enzyme in purine biosynthesis, *J. Biol. Chem.* 280, 10881–10887.
- White, R. H. (1997) Purine biosynthesis in the domain Archaea without folates or modified folates, *J. Bacteriol.* 179, 3374–3377.
- Kang, Y. N., Tran, A., White, R. H., and Ealick, S. E. (2007) A novel function for the N-terminal nucleophile hydrolase fold demonstrated by the structure of an archaeal inosine monophosphate cyclohydrolase, *Biochemistry* 46, 5050–5062.
- Murzin, A. G. (1996) Structural classification of proteins: new superfamilies, *Curr. Opin. Struct. Biol.* 6, 386–394.
- Artymiuk, P. J., Poirrette, A. R., Rice, D. W., and Willett, P. (1996) Biotin carboxylase comes into the fold, *Nat. Struct. Biol.* 3, 128–132.
- Waldrop, G. L., Rayment, I., and Holden, H. M. (1994) Three-dimensional structure of the biotin carboxylase subunit of acetyl-CoA carboxylase, *Biochemistry* 33, 10249–10256.
- Wang, W., Kappock, T. J., Stubbe, J., and Ealick, S. E. (1998) X-ray crystal structure of glycinamide ribonucleotide synthetase from *Escherichia coli*, *Biochemistry* 37, 15647–15662.
- Thoden, J. B., Kappock, T. J., Stubbe, J., and Holden, H. M. (1999) Three-dimensional structure of *N*<sup>5</sup>-carboxyaminoimidazole ribonucleotide synthetase: A member of the ATP grasp protein superfamily, *Biochemistry* 38, 15480–15492.
- Zhang, R., Skarina, T., Evdokimova, E., Edwards, A., Savchenko, A., Laskowski, R., Cuff, M. E., and Joachimiak, A. (2006) Structure of SAICAR synthase from *Thermotoga maritima* at 2.2 Å reveals an unusual covalent dimer, *Acta Crystallogr., F* 62, 335–339.
- Ginder, N. D., Binkowski, D. J., Fromm, H. J., and Honzatko, R. B. (2006) Nucleotide complexes of *Escherichia coli* phosphoribosylaminoimidazole succinocarboxamide synthetase, *J. Biol. Chem.* 281, 20680–20688.
- Matthews, B. W. (1968) Solvent content of protein crystals, *J. Mol. Biol.* 33, 491–497.
- Otwinowski, Z., and Minor, W. (1997) Processing of x-ray diffraction data collected in oscillation mode, *Methods Enzymol.* 276, 307–326.
- Vonrhein, C., Blanc, E., Roversi, P., and Bricogne, G. (2006) Automated structure solution with autoSHARP, *Methods Mol. Biol.* 364, 215–230.
- Emsley, P., and Cowtan, K. (2004) Coot: model-building tools for molecular graphics, *Acta Crystallogr., D* 60, 2126–2132.
- Brünger, A. T., Adams, P. D., Clore, G. M., DeLano, W. L., Gros, P., Grosse-Kunstleve, R. W., Jiang, J. S., Kuszewski, J., Nilges, M., Pannu, N. S., Read, R. J., Rice, L. M., Simonson, T., and Warren, G. L. (1998) Crystallography & NMR system: A new software suite for macromolecular structure determination, *Acta Crystallogr., D* 54, 905–921.
- Collaborative Computational Project-Number 4. (1994) The CCP-4 suite: programs for protein crystallography, *Acta Crystallogr., D* 50, 760–763.
- Vagin, A., and Teplyakov, A. (2000) An approach to multi-copy search in molecular replacement, *Acta Crystallogr., D* 56, 1622–1624.
- DeLano, W. L. (2002) *The PyMOL Molecular Graphics System*, DeLano Scientific, San Carlos, CA.
- Thoden, J. B., Miran, S. G., Phillips, J. C., Howard, A. J., Raushel, F. M., and Holden, H. M. (1998) Carbamoyl phosphate synthetase: caught in the act of glutamine hydrolysis, *Biochemistry* 37, 8825–8831.
- Thoden, J. B., Holden, H. M., Wesenberg, G., Raushel, F. M., and Rayment, I. (1997) Structure of carbamoyl phosphate synthetase: a journey of 96 Å from substrate to product, *Biochemistry* 36, 6305–6316.
- Thoden, J. B., Wesenberg, G., Raushel, F. M., and Holden, H. M. (1999) Carbamoyl phosphate synthetase: closure of the B-domain as a result of nucleotide binding, *Biochemistry* 38, 2347–2357.
- Fan, C., Park, I. S., Walsh, C. T., and Knox, J. R. (1997) D-alanine: D-alanine ligase: Phosphonate and phosphinate intermediates with wild type and the Y216F mutant, *Biochemistry* 36, 2531–2538.
- Hara, T., Kato, H., Katsube, Y., and Oda, J. (1996) A pseudo-michaelis quaternary complex in the reverse reaction of a ligase: structure of *Escherichia coli* B glutathione synthetase complexed with ADP, glutathione, and sulfate at 2.0 Å resolution, *Biochemistry* 35, 11967–11974.
- Yamaguchi, H., Kato, H., Hata, Y., Nishioka, T., Kimura, A., Oda, J., and Katsube, Y. (1993) Three-dimensional structure of the glutathione synthetase from *Escherichia coli* B at 2.0 Å resolution, *J. Mol. Biol.* 229, 1083–1100.

39. Holm, L., and Sander, C. (1993) Protein structure comparison by alignment of distance matrixes, *J. Mol. Biol.* 233, 123–138.
40. Morar, M., Anand, R., Hoskins, A. A., Stubbe, J., and Ealick, S. E. (2006) Complexed structures of formylglycinamide ribonucleotide amidotransferase from *Thermotoga maritima* describe a novel ATP binding protein superfamily, *Biochemistry* 45, 14880–14895.
41. Anand, R., Hoskins, A. A., Stubbe, J., and Ealick, S. E. (2004) Domain organization of *Salmonella typhimurium* formylglycinamide ribonucleotide amidotransferase revealed by X-ray crystallography, *Biochemistry* 43, 10328–10342.
42. Li, C., Kappock, T. J., Stubbe, J., Weaver, T. M., and Ealick, S. E. (1999) X-ray crystal structure of aminoimidazole ribonucleotide synthetase (PurM), from the *Escherichia coli* purine biosynthetic pathway at 2.5 Å resolution, *Structure* 7, 1155–1166.
43. Altschul, S. F., Madden, T. L., Schaffer, A. A., Zhang, J., Zhang, Z., Miller, W., and Lipman, D. J. (1997) Gapped BLAST and PSI-BLAST: a new generation of protein database search programs, *Nucleic Acids Res.* 25, 3389–3402.
44. Thompson, J. D., Higgins, D. G., and Gibson, T. J. (1994) CLUSTAL W: improving the sensitivity of progressive multiple sequence alignment through sequence weighting, position-specific gap penalties and weight matrix choice, *Nucleic Acids Res.* 22, 4673–4680.

BI701406G